

**A New Approach to Isolating External Magnetic Field Components  
in Spacecraft Measurements of the Earth's Magnetic Field  
Using Global Positioning System Observables**

Carol A. Raymond and George A. Hajj

Jet Propulsion Laboratory  
California Institute of Technology  
4800 Oak Grove Drive  
Pasadena, CA 91109

draft for *Journal of Atmospheric and Terrestrial Physics*

22 August 1994

## **Abstract.**

We review the problem of separating components of the magnetic field arising from sources in the Earth's core and lithosphere, from those contributions arising external to the Earth, namely ionospheric and magnetospheric fields, in spacecraft measurements of the Earth's magnetic field. The impact of Global Positioning System (GPS) observables (line-of-sight total electron content), obtained from high-quality GPS receivers in low-Earth orbit (LEO), on the estimation of ionospheric conductivity and current density is then considered. We demonstrate in a static data simulation experiment that accurate, high-resolution vertical profiles of electron density may be obtained for each occultation of the GPS satellite by the Earth as viewed by the LEO, and these profiles may be used to calculate conductivity distributions. We discuss the constraints these data can provide on estimating current densities in the spacecraft environment. We explore the potential of GPS electron density data, and other GPS observables such as phase and amplitude scintillations, in implementing a direct approach to estimating the external field contribution to spacecraft magnetic field observations. We conclude that while the GPS and magnetic field measurements alone may be sufficient to constrain the current distribution in the low-latitude region where the electric field is dominated by tidal forces, a more sophisticated approach is needed at high latitudes and for disturbed conditions. The simulated high latitude density profile distribution in magnetic coordinates indicates that GPS can provide significant constraints to modify high latitude conductance models. Implementing a direct estimation and removal of the external component in the spacecraft magnetic field measurements will result in better accuracy and resolution in the core field model and lithospheric anomaly field as well as produce a valuable data set of ionospheric parameters.

## **Introduction.**

Spacecraft measurements of the Earth's magnetic field are essential to producing high-accuracy main field and secular variation models. The residual field, after removal of a

degree and order 13 spherical harmonic model of the main field from the observations, contains contributions from lithospheric anomalies (sources within the Earth's crust and upper mantle), ionospheric and magnetospheric currents, unremoved core energy, and noise. The external field contribution is time-varying, a fact that is exploited in strategies for its removal, and it is strongest near the geomagnetic equator and in the auroral regions. Various methods have been utilized to achieve an effective separation of the internal (core and lithosphere) and external (ionospheric/magnetospheric current) contributions to the residual field. Although significant progress has been made in separating the lithospheric anomaly field from the external field components, certain aspects of the problem argue for a more direct approach to estimating the external field contributions. These aspects are: 1) the inadequacy of planetary magnetic indices based on ground observatory data (such as  $K_p$ ) to indicate the level of current activity in the spacecraft environment; 2) the requirement for feedback from the separation process to improve the main field model; 3) the trade-off between achieving a globally consistent lithospheric anomaly field and removing too much signal in the process; and 4) the desire to produce a high-quality, scientifically useful data set of ionospheric and magnetospheric parameters.

Here we explore the concept of using Global Positioning System (GPS) observables, namely, line-of-sight total electron content (TEC), to improve the separation of internal and external components in satellite magnetic field data. The motivation for this is twofold: 1) the inclusion of independent data on the behavior of the ionosphere and magnetosphere is needed to effect a cleaner separation of the sources that is non-destructive, i.e., that preserves the fidelity of the external field information, and 2) spaceflight-qualified GPS receivers are now available and are planned for future low-Earth-orbit (LEO) magnetic mapping missions. In the following sections, standard procedures for separating internal and external fields, and isolating the lithospheric anomaly field, are reviewed in order to clarify the aspects of the problem that could benefit from inclusion of independent data on external field behavior such as that from GPS TEC. Next, the current state and future potential of electron density

distributions derived from GPS TEC are described. Finally, a strategy for incorporating GPS TEC data into the processing stream for spacecraft magnetic field data is discussed in light of future mission opportunities.

### Separation of Internal and External Fields.

A brief review of standard methods for separating fields from sources internal and external to the Earth is presented, after Langel (1987) and Langel (1993a). Fields from sources internal to, and external to the Earth may be separated by fitting a potential function to the data of the form (Langel, 1987)

$$V = a \sum_{n=1}^{\infty} \sum_{m=0}^n \{(a/r)^{n+1} [g_n^m \cos m\phi + h_n^m \sin m\phi] + (r/a)^n [q_n^m \cos m\phi + s_n^m \sin m\phi]\} P_n^m(\cos \theta)$$

where  $a$  is the mean radius of the Earth (6371.2 km),  $r$  is the radial distance from the center of the Earth,  $\phi$  is the longitude and  $\theta$  is the geocentric colatitude.  $P_n^m(\cos \theta)$  are the associated Schmidt normalized Legendre functions of degree  $n$  and order  $m$ . At the Earth's surface, the radial field component  $B_r$  has terms of the form  $[(n+1)g_n^m - nq_n^m]$  whereas the horizontal components ( $B_\theta, B_\phi$ ) have terms of the form  $[g_n^m + q_n^m]$ . Thus, the fields may be separated analytically if well-resolved component data is available, and if the internal and external fields are organized in the same coordinate system (Langel, 1993a). For satellite magnetometers in low Earth orbit, the ionospheric fields are dominantly internal to the satellite's orbit. A potential function that fits the data in a dipole latitude/local time coordinate system may be used to isolate the ionospheric contributions if the data has an adequate distribution in local time, but the typical low altitudes of magnetic field satellites does not allow the contributions of the currents themselves to be separated from the induced Earth currents based on the attenuation characteristics. The presence of field-aligned currents in the spacecraft environment causes the underlying assumption of a curl-free magnetic field to break down, invalidating the use of

potential functions to describe the fields. Thus, at high latitudes, where field-aligned currents are frequently present, only the vertical component or field magnitude is used to represent the internal portion of the field, since it is little affected by these currents (Langel, 1974; 1987).

Coefficients of the external portion of the field,  $q_1^0$ ,  $q_1^1$  and  $s_1^1$  reflect the strength of the magnetospheric ring current, which has a relatively simple morphology that is symmetric about the Earth's dipole axis, and the magnetospheric tail current and magnetopause current. These coefficients have been determined in an analysis of Magsat data (Langel et al., 1980; Langel and Estes, 1985) where they were considered functions of the magnetospheric ring current index  $D_{st}$ , thus accounting for their universal time variations. Magsat was launched by NASA on October 30, 1979 into a 578 by 352 km sun-synchronous, dawn-dusk polar orbit; it operated for 6 months and was the first magnetic field satellite dedicated to measuring the main and lithospheric anomaly fields. It carried a fluxgate vector and cesium vapor scalar magnetometer, and used star cameras to resolve attitude to several tens of arc-secs.

The much greater temporal and spatial variability of ionospheric currents, as well as their distribution both internal (electrojet,  $S_q$ ) and external (field aligned, meridional) to low-Earth orbit requires high-quality vector data collected at all local times over at least one seasonal cycle in order to derive accurate higher-order coefficients describing their contributions. The ionospheric current contributions have a strong local time and seasonal dependence which facilitates their characterization. A study by Yanagisawa and Kono (1985), and more recent studies by Cohen and Achache (1990), Langel et al. (1993b) and Ravat and Hinze (1993), have extracted empirical estimates of the equatorial electrojet contribution in Magsat data by analysing the residual quiet-time data in dip-latitude and local time coordinates. A clear electrojet current (and meridional current) contribution was recognized in the dusk data, while the dawn data were apparently largely free of such contamination (Langel et al., 1993b; Ravat and Hinze, 1993). Equivalent current systems (at dusk local time) calculated from the residual component data for two month sections revealed a systematic seasonal morphology and longitudinal amplitude variation (Langel et al., 1993b). Thus, six months of Magsat vector

measurements, with an accuracy of  $\sim 6$  nanoteslas per component, appear to be sufficient to define the first-order characteristics of the morphology and variability of the equatorial electrojet and associated meridional currents, even though the measurements are concentrated at dawn and dusk local time.

Spacecraft vector magnetic field measurements, collected over all local times several times during a seasonal cycle, would facilitate the separation of systematic (quiet-time) external fields from the crustal field on the basis of their local time dependence. However, the ability to characterize the external current contributions using data from a single spacecraft collected over a time period of one year, which is the targeted lifetime of many planned magnetic field missions, is limited. The variability of the disturbance level of the field in single spacecraft data compromises the distribution of the data over all local times, and the complex morphology of the auroral fields confounds their characterization by empirical or theoretical models. Thus, either the quiet time data alone can be used to derive a first-order estimate of the current strength and morphology (for equatorial and mid-latitudes) with local time and seasonal dependence, or the intense variability of the current systems during disturbed periods can be examined, but without an understanding of the global strength and morphology of the current systems. Ideally, we seek an approach where all signals may be sorted according to their sources such that the residuals approach the measurement error. This scenario would not only improve the accuracy of all derived component fields, but would improve the recovery of global conductivity variations through knowledge of the source function (ionospheric current) and response (induced currents in Earth).

### **Isolation of the Lithospheric Field.**

Next, we present a brief review of some common procedures used to isolate the lithospheric field in Magsat residual data (after removal of the degree and order 13 main field model). The most common first step is to assemble a set of passes collected during quiet times, defined as times when the  $K_p$  index is below a threshold value, most commonly two.

Passes with spikes exceeding a threshold (20 nT) are considered suspect and discarded. The remaining passes are then detrended with a first- or second-order polynomial (linear or quadratic fit). Frequently, the data are split into subsets based on local time (for Magsat, dawn or dusk). The dawn and dusk data sets are treated independently, and comparisons are used to identify components that vary in local time and are therefore considered not of crustal origin and discarded. There have been many variations on the last step, two of which are discussed in more detail below. The discussion is intended to be instructive rather than exhaustive.

In the analysis of Arkani-Hamed and Strangway (1985; 1986), a quiet time data set was assembled from which a degree and order 13 main field model and then a magnetospheric ring current model were removed; a quadratic function was then fit and discarded for each residual pass. Spherical harmonic representations of the dawn and dusk data sets were derived, and the symmetry evaluated between the two data sets for all harmonic components. The anti-variant and contaminated co-variant harmonics of the two data sets, identified on the basis of degree correlation coefficients, were eliminated by application of a bandpass filter in the spherical harmonic domain (harmonics  $n=m=18$  to 41), in order to remove the remaining external field components and noise at higher harmonic degree. It is suspected that a considerable amount of lithospheric anomaly field energy at long wavelength (above  $\sim 2200$  km) was lost because of the strong influence of the external current systems for degrees 15 and 17.

Subsequently, Arkani-Hamed et al. (1994) used spherical harmonic degree correlation coefficients to isolate the co-variant harmonics of the ionosphere-corrected Magsat dawn and dusk maps of Ravat et al. (1994) and a newly derived POGO (Polar Orbiting Geophysical Observatory) anomaly map at 400 km (Langel, 1990). They produced two maps, one for harmonics 15-60 and the other 15-65; the restricted range of harmonics contains a higher signal-to-noise ratio but reduced signal power. Ravat et al. show, by comparison of a power spectrum of the filtered fields to the predicted natural spectrum of the internal field (Cain et al., 1989), that significant signal power associated with the internal field has been lost in the process of suppressing the external field contributions in the data. In particular, they conclude

that along-track filtering has removed crustal signal in the spectral range of degrees 15-24, while the ionospheric corrections have reduced power further, up to degree 40. Therefore, while these techniques have greatly enhanced the accuracy of the lithospheric anomaly field in the satellite data, significant information has been destroyed, particularly in the low-order harmonics which cannot be reliably sampled by any other means.

An analysis of Magsat data in the south polar region by Alsdorf et al. (1994) has refined the assessment and removal of differences between the dawn and dusk polar data sets. Alsdorf et al. (1994) have applied a Fourier wavenumber correlation filter iteratively to retain coherent wavenumber components of adjacent polar passes. The data were first despiked, then a core field model, to which a first-order levelling adjustment was made, was removed. The data were then split into dawn and dusk components, and into four altitude bins for each local time. All passes were filtered, regardless of the level of external field activity; however, passes with high variance were eliminated from further analysis. Application of the correlation filter increased the correlation coefficients of each data subset substantially. Equal-area grids of the eight subsets were constructed by least-squares collocation. The dawn and dusk grids at each altitude were then filtered for their correlative wavenumber components and their correlated components were combined to produce a grid of the common features of the data set. This was done for each altitude and the four maps at different altitudes were continued to a common altitude of 430 km by equivalent point source inversions. The final grid at 430 km is a product of a final correlation filter step that retains those components common to all the altitude bins. This method appears to have produced a highly self-consistent lithospheric anomaly data set.

#### **Discussion of the Separation Problem.**

There are several common procedures in the previously described analyses which compromise the information contained in the original data. The most common of these is to remove a linear or quadratic fit to each individual pass after the main field model has been

removed. This detrending removes remaining long-wavelength core field and external field energy, which is then lost from subsequent analysis. The ability to organize the long-wavelength residuals to separate the likely contribution of the magnetospheric and solar quiet variations from the errors in the core field model would allow the possibility of feeding back information to improve the core field model.

Extraction of the lithospheric anomaly field also suffers from three other problems: 1) the inability of the  $K_p$  index (or  $AE$  index) to characterize the level of ionospheric activity in the polar regions, and to some extent in the equatorial and mid-latitudes; 2) the ambiguity in determining the "quiet time" field magnitude in separation procedures that utilize the local time dependence of external fields; and 3) the "lowest common denominator" characteristic of filtering to reduce external field noise. The  $K_p$  index is constructed as a weighted average of the disturbed horizontal component of the magnetic field (relative to a quiet value) at 12 mid-latitude observatories. It does not reflect the activity in the auroral zones, except when that activity affects the mid-latitude stations by expansion of the auroral zone. Likewise, variations in the strength of the equatorial electrojet are not well-represented by the disturbances recorded at mid-latitude stations. Since  $K_p$  is a planetary index, it is useful in evaluating probable contamination on a pass which samples a hemisphere, but it is insufficient to screen out passes contaminated only at high and low geomagnetic latitude. The second problem concerns the bias which may result when quiet time data collected at different local times are compared in order to isolate the time-varying portion of the field. This procedure assumes that one knows which field is quieter than the other. In reality, each data set is contaminated to a different degree, which complicates the interpretation of the difference field in terms of distinct ionospheric sources. The last item, the "lowest common denominator" characteristic, is perhaps the most problematic, and is discussed below.

The objective of the techniques of Arkani-Hamed and Strangway (1985; 1986), Arkani-Hamed et al. (1994) and Alsdorf et al. (1994) is to extract a spatially correlated signal from a temporally varying one. This is achieved by filtering in the spherical harmonic domain and

the fourier wavenumber domain, respectively. The filtering undoubtedly removes to a large degree the external field noise, along with any lithospheric signal that is contained in the same band. Thus, in order to produce a globally consistent lithospheric anomaly field free of external field contamination, Arkani-Hamed and Strangway and Arkani-Hamed et al. (1994) had to discard all signal in bands dominated by noise, whether or not the individual passes were contaminated. Alsdorf et al. assume that the correlated portion of the signal in adjacent passes (which are separated in time) is lithospheric in origin and the uncorrelated portion is noise. They used a correlation coefficient of .3 as a cutoff in order to preserve a reasonable level of signal power, illustrating the overlap in the signal and noise spectra. The iterative application of their filter resulted in gradually increasing signal-to-noise ratios as well as decreasing signal power. The power in the resulting set of dusk-data-only grids for the four altitude bins was approximately twice that of the corresponding dawn maps. This underscores a problem in the isolation of the fields by this method. The dawn and dusk grids for each of the four altitude bins were averaged to produce the final grid at each altitude. The ambiguity in the proper signal level between the two maps, and the possible introduction of spurious anomalies caused by variation of the signal level within a single map, leads to uncertainty in the final maps produced by this method.

Current plans for low-Earth orbiting magnetic field mapping missions call for a circular orbit precessing in local time such that all local times are sampled on the order of three times per year over three years (e.g. Gravity and Magnetic Earth Surveyor [GAMES] Frey, 1993) or an elliptical orbit precessing six hours over one year (e.g. Ørsted; Friis-Christensen, pers. comm). While a precessing orbit is an improvement over the sun-synchronous orbit of Mag-sat, the desire to keep the orbital inclination as high as possible tends to entwine the seasonal dependence of the time-varying fields with the local time dependence; the Ørsted orbit does not sample all local times, but is restricted to the statistically quietest local times. In an ideal scenario where two or more satellites are orbiting at different local times, and preferably different altitudes, for at least one seasonal cycle, the strength of the magnetic field data alone

should be sufficient to separate the external fields from those of the core and lithosphere. Until this scenario is realized, the problems described above remain, and we must seek a means to organize the magnetic field data such that the external sources may be identified with greater confidence. The inclusion of electron density estimates derived from GPS observables is discussed below in this context. Although electron density can only provide indirect information about current activity and the resulting magnetic disturbance fields in the spacecraft environment, the availability and density of GPS electron density data provides a strong motivation for utilizing these data in the magnetic data processing stream. GPS has great promise as an efficient and cost-effective means to characterize the ionosphere, and GPS receivers are planned for future geomagnetic missions.

#### Global Electron Density from GPS.

As a result of their interaction with free electrons along the propagation path, GPS signals traversing the ionosphere experience a frequency-dependent group delay (and phase advance) relative to propagation in a vacuum. Because of the dominance of the  $f^{-2}$  component of this delay, dual-frequency GPS signal group delays yield an absolute measure of the total electron content (TEC) along the line-of-sight (los) between the satellite and receiver. The precision of the absolute TEC measurement with a high performance receiver is about 1 TEC unit ( $1 \times 10^{16}$  electrons/m<sup>2</sup>), even when anti-spoofing (AS) is in effect (Srinivasan et al., 1989). The phase advance yields relative TEC to much greater precision (.01 TEC units). Data from a network of ground receivers may be combined to yield maps of global electron density at intervals of one hour (Wilson et al., 1993; Mannucci et al., 1993); these maps display vertically-integrated electron density because data from the ground are not sensitive to vertical structure in the ionosphere (Raymund et al., 1990; Yeh and Raymund, 1991; Hajj et al., 1993). Data taken in an occulting geometry from a LEO spacecraft, as illustrated in Fig. 1, may be combined with data from a network of ground receivers to perform a tomographic inversion that reveals both horizontal and vertical variations in electron density (Raymund et

al., 1993, 1994; Hajj et al., 1994). The estimated maximum vertical and horizontal resolution of a tomographic inversion which includes data from one LEO spacecraft is about 300 km in the horizontal and 45 km in the vertical (Hajj et al., 1993). Clearly, while the estimates of global electron density derived from tomographically inverted GPS data are valuable, they cannot reveal the structure of the E region, and therefore would not furnish strong constraints on estimating the strength and morphology of ionospheric current systems. However, the combined ground and LEO data may be used to derive vertical profiles of electron density at the tangent point of the occultation, for which the vertical resolution is set by the first Fresnel zone, which is approximately 1 kilometer. These vertical profiles are discussed in the next section.

The global electron density distributions obtained from combined LEO/ground data are potentially valuable for monitoring large scale changes in the magnetosphere which result from injections of plasma from the solar wind and precede vigorous storm activity in the ionosphere. Electron precipitation in the auroral zones will appear as an increase in electron density, and the energy level of the precipitating electrons may be derived from the height to which they penetrate in the ionosphere, raising the possibility of obtaining energy distributions of the precipitating electrons with respect to height. These estimates are limited to a temporal resolution on the order of the orbital period, about 90 minutes. The global 3-D electron density, while not directly applicable to the estimation of current densities in the E-region, could be useful as a proxy for the level of activity in the ionosphere, complementary to the magnetic activity indices obtained from ground magnetic observatories. The value of the global electron density measurements is enhanced by their absolute nature, and their fine spatial resolution relative to the sparsely distributed magnetic observatories.

#### **Local electron density measurements from spacecraft occultations.**

Vertical profiles of electron density with one kilometer resolution and accuracy of <1 TEC unit may be obtained by combining spacecraft occultation data and data from a GPS

ground network. These profiles are resolved at the tangent point of the occultation. The number of occultations each day for a single spacecraft antenna is over 200. A representative daily distribution of occultations for the GPS-MET satellite (with aft-looking antenna) is shown in Figure 2. GPS-MET is an experimental satellite scheduled for launch in September 1994 that will obtain occultation data primarily for atmospheric temperature and moisture profiles. A second antenna to capture occultations in the forward direction would double the number of profiles obtained.

Hajj et al. (1994) obtained simulated density profiles by propagating dual-frequency GPS signals through a model ionosphere to a low-Earth orbiting spacecraft in an occultation geometry; data from a network of ground receivers were also included to constrain horizontal variations in density. The electron density model was derived from the Parameterized Ionosphere Model (PIM) developed by D. N Anderson of the Air Force Phillips Laboratory. In their experiment, an electron density model corresponding to daytime, solar max conditions [1200 UT; 20°E longitude; September 26, 1992] was used. No dynamic behavior is included in the model. Sample profiles from Hajj et al. (1994) are shown in Figure 3 for four latitudes: 20°S, 0°, 20°N and 40°N; open square symbols represent the profile recovered from the occultation data alone, and filled squares the profile derived by including constraints from ground data. Comparison of the profiles recovered from analysis of the simulated GPS signals to the model input reveals that: 1) while the general shape of the profiles is usually well-reproduced, the recovered densities often deviate significantly from the input; and 2) the profiles at 0° and 20°N underestimate the F-region peak density, while at 40°N the peak density is overestimated. This behavior is caused by the location of the peak density at ~20°N. For occultations with tangent points at 20°N, the signal will be slower on either side of the tangent point, causing the estimate to be too small. In the general case where the tangent point represents neither a maximum nor a minimum in density, but is characterized by a linear gradient, the signal speeds up and slows down by equal amounts on either side of the tangent point, resulting in a more accurate density estimate. Such is the case for 20°S, shown

in Fig 3a. For a profile near a minimum in density (40°N), the recovered density is too large. To eliminate this problem, solutions may be obtained iteratively using the information from nearby profiles to help characterize the density gradients that the signal encounters. These vertical electron density profiles can constrain the dynamics of the ionosphere and strength and morphology of the current systems in several ways.

### Conductivity and Current Density Estimates.

The vertical profiles provide E region density estimates, which yield estimates of conductivity,  $\sigma$ , by appropriate substitutions in the following equations: (Kelley, 1989)

$$\sigma_o = ne (b_i - b_e)$$

$$\sigma_p = ne [b_i / (1 + \kappa_i^2) - b_e / (1 + \kappa_e^2)]$$

$$\sigma_H = (ne/B) [\kappa_e^2 / (1 + \kappa_e^2) - \kappa_i^2 / (1 + \kappa_i^2)]$$

where  $b_j = (q_j/M_j v_{jn})$  is the mobility,  $\kappa_j = (q_j B / M_j v_{jn})$  is the ratio of gyrofrequency to collision frequency,  $B$  is the magnetic field strength,  $q_j$  is the elemental charge,  $M_j$  is the electron or average ion mass,  $v_{jn}$  is the ion-neutral or electron-neutral collision frequency, and subscripts  $e$  and  $i$  refer to electron and ion, respectively. The electron-neutral collision frequency may be approximated as

$$v_{en} = (5.4 * 10^{-10}) n_n T_e^{1/2} s^{-1}$$

where  $n_n$  is the neutral density and  $T_e$  is the electron temperature. The ion-neutral collision frequency is given by

$$v_{in} = (2.6 * 10^{-9}) (n_n + n_i) A^{-1/2} s^{-1}$$

where  $A$  is the average molecular weight of the plasma.

The three conductivity components are the parallel ( $\sigma_o$ ), Pedersen ( $\sigma_p$ ) and Hall ( $\sigma_H$ ). The parallel component is aligned with the direction of the Earth's magnetic field, the

Pedersen conductivity is aligned with the electric field, and the Hall conductivity is perpendicular to both the magnetic and electric fields. At the equator, the horizontal magnetic field geometry creates a barrier to vertical Hall current flow, resulting in a vertical polarization electric field. The polarization electric field augments the zonal conductivity, which creates an intense zonal current jet, known as the equatorial electrojet. The equatorial electrojet, whose strength and morphology are controlled by tidal winds in the E region, flows eastward during the day and westward at night. The zonal conductivity near the equator is  $[1 + \sigma_H^2 / \sigma_P^2] \sigma_P$ , which is the Cowling conductivity,  $\sigma_c$ . First-order current density estimates for the equatorial electrojet may be obtained by calculating the Cowling conductivity from GPS electron density and model values of neutral density, average molecular weight and electron temperature and assuming a zonal electric field strength.

*Equatorial electrojet current density estimates.*

In the equatorial E region, the large difference in the scale size of the horizontal and vertical variations in conductivity (horizontal scale 100 times the vertical scale) results in a nearly invariant zonal electric field; thus, the divergence of the Hall current, and therefore the equatorial electrojet strength, is dominated by the conductivity gradients (Kelley, 1989). For this reason, we restrict our calculation of current density to the equator.

Estimates of electron density derived from GPS observables can provide significant constraints on the conductivity of the E region, and also map the temporal and spatial variability in greater detail than can be obtained by existing methods which obtain discrete samples widely separated in space and time (such as rocket flights or incoherent scatter radar), or other beacon satellites that lack the robustness of the GPS constellation. The errors on the reconstructed E region vertical profiles are small when the density gradient is smooth, as is the case for 40°S (Figure 4), obtained in the simulation described above. Near the equator, where the density gradients are severe, and proximal to the equatorial anomaly at 20°N (Fig. 3c), the recovery is worse. No constraints were imposed in the inversion that the recovered density be

positive, and the simulated profiles shown in Figure 3b, c, and d all show negative densities at the base of the E region, an obviously physically unrealistic result. We therefore removed a bias from the profiles so that they were zero at their minimum points. Removal of the bias leads to the remarkable agreement between the true and reconstructed profiles, as shown in Figure 5 (a, b, c) for geomagnetic latitudes of  $10^{\circ}\text{S}$ ,  $0^{\circ}$  and  $10^{\circ}\text{N}$ . While this adjustment is ad hoc, it reflects the accuracy we expect to obtain by imposing a positivity constraint on the recovered density profile.

Shown in the middle panels of Figure 5 are conductivity estimates  $\sigma_o$ ,  $\sigma_H$ ,  $\sigma_P$ , and  $\sigma_c$  derived from the GPS electron density estimates. The Cowling conductivity,  $\sigma_c$ , computed from the starting model density profile is shown for comparison. Zonal current densities are calculated by multiplying the Cowling conductivity profile by a zonal electric field value of .5 mV/m, an average equatorial value (Woodman, 1970; Kelley, 1989). The results, shown in the far right panels, indicate excellent agreement between the model-derived and GPS-derived current density profiles. In particular, it is encouraging that the maximum agreement between the model and reconstructed density profiles in the E region occurs near the density maximum. The conductivity estimates are most accurate where the gradients are largest.

The current density estimates are derived by assuming a constant zonal electric field,  $E_x$ , in the equatorial region appropriate to noon local time. In reality, when calculating a time series of current density estimates, a model including the diurnal and semidiurnal variations, as well as seasonal variations in  $E_x$  (Woodman, 1970; Balsley and Woodman, 1971; Balsley, 1973; Fejer et al., 1979; Richmond et al., 1980; Fejer, 1981) would be employed. The use of an average electric field model, appropriate for the latitude and solar cycle position, would not contribute a large error to the estimated current densities in the equatorial and mid-latitude E region for quiet times. However, the penetration of auroral electric fields to the equatorial region during magnetically disturbed conditions (Onwumechili et al., 1973; Gonzales et al., 1979) would result in large errors in the current density estimates. Fortunately, large excursions in  $E_x$  caused by the influence of magnetospheric electric fields would be recognizable in

the electron density data as an increase in the height of the density maximum ( $h_{\max}$ ) caused by upward plasma flow (e.g. Behnke et al., 1985). Although the GPS density profiles can provide an indication of the gradients in the electric field, the data cannot constrain the field magnitude nor track the rapid fluctuations during disturbed conditions. It would therefore be difficult to obtain current density estimates for the equatorial electrojet during such times without independent information on the electric field.

### *High-Latitude Conductivity and Electrodynamics.*

High-latitude electrodynamic are considerably more complex than those in the equatorial region. At high latitudes, the conductivity is dominated by electron and ion precipitation from the solar wind, and the electric field is highly dynamic. In addition, the magnetic field geometry and presence of field-aligned currents preclude the application of simplifying assumptions about the current distribution. Thus, periodic density profiles from GPS provide insufficient constraints on the strength and morphology of the current systems there. Direct knowledge of vector plasma drifts (electric field) and electron precipitation that alters conductivity is also necessary to estimate currents. Sophisticated methods of merging all available data with statistical models to estimate electrodynamic in the polar ionosphere have been developed; these efforts have culminated in the Assimilative Mapping of Ionospheric Electrodynamics (AMIE) scheme which fits the ionospheric electrodynamic parameters to the data and assigns quantitative uncertainty estimates to the derived parameters (Richmond and Kamide, 1988; Richmond et al., 1988; Knipp et al., 1989; Richmond, 1992).

AMIE relies on statistical conductivity models (Fuller-Rowell and Evans, 1987) scaled by the Hemispheric Power Index (HPI) derived from particle precipitation data along NOAA 6, 7 and 8 and DMSP F-7 satellite orbits (Foster et al., 1986) to constrain ionospheric conductance. Richmond et al. (1988) observed discrepancies between the model predictions of conductance and that calculated directly from incoherent scatter radar (ISR) density measurements. They demonstrated the improvement in the derived electrodynamic parameters that

resulted when the ISR conductivity estimates were included to modify the conductance model. Ground magnetometer observations are also used to improve the conductance model; however, the errors in this method are large, especially for low conductance. GPS occultation measurements in the polar regions offer the possibility of greatly expanding the database of conductivity measurements and reducing uncertainty in the calculated current distributions. Figure 6 shows the predicted distribution of occultations obtained during one day in a simulated orbit of the Danish Ørsted geomagnetic satellite for northern and southern polar regions in magnetic coordinates. The symbols represent the tangent points of the occultation ray paths (the points of maximum penetration), where the high-resolution vertical density profiles are resolved. These plots indicate the greater number and better distribution of high-resolution density profiles that can be recovered with GPS each day in the polar regions, relative to ISR, to constrain conductance.

#### **Application to the Magnetic Field Separation Problem.**

In the previous section, we have shown the potential of GPS electron density to provide accurate conductivity estimates, and current density estimates for the equatorial electrojet based on an electric field model. We chose to start with a model of the equatorial electrojet because the unique orientation of the magnetic field there simplifies the physics and allows us to calculate first-order current densities with greater confidence than in the mid-latitudes or the auroral region. Although the estimates of conductivity will be fairly robust, estimating global current densities in the E region from GPS electron density will be considerably more challenging in a dynamic environment than in the static example we present here. There are several problems to overcome or work around in developing methods to utilize constraints from GPS in analyzing magnetic field data. The most serious of these is characterizing the dynamic behavior of the electric field, which, along with the conductivity controls the strength and distribution of currents. Another important problem is dynamic behavior in the ionosphere during the time required to obtain an occultation, which may seriously compromise the

recovery of accurate vertical density profiles. However, since the magnetic field data itself is directly measuring the disturbance fields produced by the currents, the problem is reduced to combining the strengths of the GPS and magnetic data to estimate the current strength and distribution.

Electric field models are valid for latitudes and local times for which the electric field is dominated by tidal forces. At times when the magnetosphere exerts influence on the electric field, the models break down. Yet it is precisely at these times that we would like to understand the currents in order to separate the magnetic disturbance fields resulting from the currents from fields generated in the Earth. Aside from incorporating electric field data from independent sources, we have two means of recourse for understanding the behavior of the electric field from GPS data alone. First, as mentioned above, the height of the F region density peak,  $h_{\max}$ , indicates the balance between upward plasma flow driven by the eastward electric field and gravitational forces that resist such flow. Changes in  $h_{\max}$  that are not consistent with tidal wind models would then reflect external forcing of the electrodynamics by imposed magnetospheric fields. Magnetospheric forces dominate the electrodynamics of the auroral zone, whereas tidal forces are predominant at low and mid-latitudes. Thus  $h_{\max}$  from the accurate vertical density profiles will provide a means to distinguish periods when electric field models are valid (quiet times). It will also provide some information to classify the magnetic data with regard to the relative contribution from external fields expected along any given pass.

The low-latitude electric field is strongly affected by magnetospheric and high-latitude electric fields during disturbed conditions (Matsushita and Balsley, 1972; Onwumechili et al., 1973; Fejer et al., 1976, 1979; Gonzales et al., 1979). Because tidal electric field models are invalid in high-latitude regions, an approach such as AMIE that directly estimated the electric field from available data would be required to accurately estimate the current distribution there. Knowledge of the electric field at high-latitude would also provide a useful constraint on the low-latitude electric field behavior during disturbed conditions, and could be used

along with the density and magnetic field data to estimate the electric field and current distribution there.

In addition, inhomogeneities in the electron density along the GPS signal path ( $\delta N / N$ ) act as a diffraction screen, causing the phase and amplitude of the signal to scintillate. For a thin-screen, weak-scattering approximation, the power spectrum of the scintillations is a linearly filtered version of the power spectrum of the density fluctuations (irregularities); they are related by the Fresnel filtering factor, which is a function of the height of the irregularity layer and the frequency of the signal (Salpeter, 1967; Rufenach, 1971). Deep minima in the scintillation power spectrum result from the Fresnel filtering factor and can be used to estimate the velocity of the irregularities (e.g. Rufenach, 1972), which has been shown to be equal to the electron drift velocity by correlation with ground magnetic perturbations (Rastogi et al., 1972). L-band GPS signals are sensitive to irregularities of one-half kilometer or smaller in size. Autocorrelation and cross-correlation of signals from an array of receivers can also be used to estimate the drift velocity of irregularities (e.g. Briggs, 1977, 1980; Basu et al., 1991). Scintillation data from a network of GPS receivers strategically placed on the ground would be a valuable asset for estimating electron drift velocity at the F peak for constraining the electric field.

The problem of dynamic behavior in the ionosphere during an occultation, which would typically last a few minutes, is one that has no clear solution. However, our ability to recognize that the density structure along the propagation path is varying on the time scale of the measurement is a powerful observation in itself, and indicates to some extent the level of activity in the ionosphere. The 50 Hz sampling rate and robust tracking loop of the modified TurboRogue spaceborne GPS receivers should mitigate this potential problem.

#### *Approaches to Estimating Current Distributions.*

The most basic scenario for synergistically combining the GPS and magnetic field data collected from an LEO satellite, is to use the GPS TEC to devise a means to classify the

expected level of external magnetic field activity for individual passes. Then, a quiet time field could be derived from those passes deemed to have been collected during very magnetically quiet periods on the basis of GPS conductivity estimates, variations in global electron density distribution (from tomography) and  $h_{\max}$  from GPS, as well as  $K_p$ . Residuals to the main field model constructed from these quiet passes would be analyzed for correlation between anomaly strength and GPS parameters to identify quasi-static unremoved external field components. Contaminated passes could then be analyzed relative to this quiet field, and weighted according to their relative tidal (diurnal, semidiurnal) versus magnetospheric (impulsive) affinities, to derive the morphology of the external field.

A more sophisticated approach is to combine the two data types directly in a parameter estimation scheme. In this approach, current density distribution in the equatorial and mid-latitude regions would be estimated directly from the GPS-derived conductivities and an electric field model, combined with constraints from the satellite magnetic field data referenced to an *a priori* quiet (core and lithospheric) model. The resulting fit would utilize the strength of both data sets and exploit their synergism. Analysis of subsets of the residual data, organized by season and/or local time, would add further constraints on the extraction of the static lithospheric anomaly field. A parameter estimation approach would also allow the electric field to vary from the *a priori* statistical model within the available constraints, and be fit as an additional parameter. Available constraints include  $h_{\max}$  and its temporal gradient, high-latitude electric field, IMF direction and periodic electric field model updates obtained by independent data or GPS phase scintillations.

As discussed above, AMIE is the most appropriate approach for estimating the current density distribution (and other parameters) in the polar ionosphere. Incorporation of high-resolution GPS density profiles and lower resolution global electron density into AMIE would reduce the uncertainties and improve the resolution of the estimated current distributions. The challenge we face in implementing these direct approaches is to develop a scheme that is efficient enough, and eventually automated, to allow a cost-effective analysis of large volumes

of satellite magnetic field data collected over months or years.

Successful direct estimation of current distributions has several implications for solid Earth magnetic field investigations. Removal of the estimated external  $\Delta B$  component from each satellite pass prior to modeling the core component would improve the core field recovery, and would raise the possibility of including full vector measurements at high-latitude in the model instead of only  $\Delta Z$  if the correction is accurate enough. This would be an iteration on the field model that was calculated initially to estimate an *a priori*  $\Delta B$  for input to the fitting procedure for the current density distribution. Residuals of the improved core-field model could then be considered to be lithospheric in origin and combined using the filtering techniques described above to produce high-quality, full-resolution anomaly fields. One goal is to omit the along-track filtering which is done to suppress residual core field error and external contamination in the compilation of the anomaly fields. The effects of along-track filtering on the accuracy of the resultant anomaly fields is unknown, but it is clear that power and resolution are lost in this step. An additional benefit of removing the external component first is that the induced Earth currents are also removed, which helps to equalize the power in the internal fields between disturbed and quiet times or two different local times. The other obvious benefit of this scheme is an uncorrupted data set of ionospheric parameters with greater precision that will be valuable for examining the temporal and spatial variability of ionospheric processes in a continuous fashion.

#### Future Directions.

As shown here, the recovery of E region electron density with height from GPS occultation data is very accurate and the data distribution is spatially and temporally robust. Imposing positivity on the solution (to avoid the removal of the negative bias), and iterating the solution with updated information on horizontal gradients obtained from the occultation data itself, will improve the absolute recovery and agreement with the model input. These modifications to the retrieval algorithm will be incorporated in the near future. The

availability of occultation data from GPS-MET, and an expanded GPS ground network will allow us to compute hundreds of GPS-derived electron density profiles per day with great accuracy and fine vertical resolution. Additional orbiting receivers, proposed for several planned missions, including the Danish Ørsted geomagnetic satellite, may increase the number of daily profiles to over one thousand per day and densify the global coverage.

Although the primary inference that can be drawn from analysis of dual-frequency GPS signal propagation through the ionosphere is the variation in electron density, such knowledge can be gainfully applied to sensing the dynamics of the ionosphere as well. Making simple assumptions, we can globally map coarse variations in the conductivity distribution over time scales of 1-2 hours, and we can define conductivity profiles at discrete points very accurately. The shape of the density gradients and height of the density peak reveals information about the dynamics of the plasma and electric field. GPS scintillation measurements also offer a valuable resource for sensing ionospheric dynamics, including the nature of turbulent instabilities. Combining GPS observables from ground and spacecraft data with satellite magnetic field data has great potential to increase the value of satellite magnetic field data to both solid Earth and ionospheric investigations and perhaps narrow the gap between these disciplines by producing an integrated data set characterizing the magnetic environment of the Earth.

**Acknowledgments.** This work has benefited from discussions with Rob Kursinski, Tony Mannucci, Bob Langel, and Art Richmond. This work was carried out at the Jet Propulsion Laboratory under contract with the National Aeronautics and Space Administration. Support from the JPL Director's Discretionary Fund and NASA RTOPs 465-13-06-04 and 465-35-02-01 is gratefully acknowledged.

References.

- Alsdorf, D.E., R.R.B. von Frese, J. Arkani-Hamed, and H.C. Noltimier, Separation of lithospheric, external and core components of the south polar geomagnetic field at satellite altitudes, *J. Geophys. Res.*, *99*, 4655-4668, 1994.
- Arkani-Hamed, J. and D.W. Strangway, Magnetic susceptibility anomalies of the lithosphere, *J. Geophys. Res.*, *90*, 2655-2664, 1985.
- Arkani-Hamed, J. and D.W. Strangway, Band-limited global scalar magnetic anomaly map of the Earth derived from MAGSAT data, *J. Geophys. Res.*, *91*, 8193-8203, 1986.
- Arkani-Hamed, J., R.A. Langel, and M.E. Purucker, Scalar magnetic anomaly maps of Earth derived from Pogo and Magsat data, *J. Geophys. Res.*, *99*, in press, 1994.
- Balsley, B. B., Electric fields in the equatorial ionosphere: a review of techniques and measurements, *J. Atmos. Terr. Phys.*, *35*, 1035-1044, 1973.
- Balsley, B. B., and R. F. Woodman, On the control of the *F* region drift velocity by the *E* region electric field: Experimental evidence, *J. Atmos. Terr. Phys.*, *31*, 865, 1973.
- Behnke, R. A., M. Kelley, C. Gonzales, and M. Larsen, Dynamics of the Arecibo ionosphere: A case study approach, *J. Geophys. Res.*, *90*, 4448, 1985.
- Bhattacharyya, A. and R. G. Rastogi, Structure of ionospheric irregularities from amplitude and phase scintillation observations, *Radio Science*, *26*, 439-449, 1991.
- Briggs, B. H., Ionospheric drifts, *J. Atmos. Terr. Phys.*, *39*, 1023-1033, 1977.
- Briggs, B. H., Radar observations of atmospheric winds and turbulence: a comparison of techniques, *J. Atmos. Terr. Phys.*, *42*, 823-833, 1980.
- Cain, J. C., Z. Wang, D. R. Schmitz, and J. Meyer, The geomagnetic spectrum for 1980 and core-crustal separation, *Geophys. J. R. Astr. Soc.*, *97*, 443-447, 1989.
- Cohen, Y., and J. Achache, New global vector magnetic anomaly maps derived from Magsat data, *J. Geophys. Res.*, *95*, 10783-10800, 1990.
- Fejer, B. G., C. A. Gonzales, D. T. Farley, M. C. Kelley and R. F. Woodman, Equatorial electric fields during magnetically disturbed conditions, 1, The effect of the interplanetary magnetic field, *J. Geophys. Res.*, *84*, 5797, 1979.
- Fejer, B. G., D. T. Farley, B. B. Balsley and R. F. Woodman, Radar studies of anomalous velocity reversals in the equatorial ionosphere, *J. Geophys. Res.*, *81*, 4621, 1976.
- Fejer, B. G., The equatorial ionospheric electric fields. A review, *J. Atmos. Terr. Phys.*, *43*, 377-386, 1981.
- Foster, J. C., J. M. Holt, R. G. Musgrove, and D. S. Evans, Ionospheric convection associated with discrete levels of particle precipitation, *Geophys. Res. Lett.*, *13*, 656-659, 1986.
- Frey, H., J. Abshire, B. Bills, J. Connermey, B. Johnson, R. Langel, F. Lerch, S. Nerem, E. Pavlis, D. Skillman, D. Smith, P. Taylor, and C. Voorhies, GAMES: A Gravity and Magnetism Experiment Satellite for Oceanography and Solid Earth Science, *EOS, Trans. AGU*, *74*, Spring Meeting Suppl., *97*, 1993.
- Fuller-Rowell, T. J., and D. S. Evans, Height-integrated Pedersen and Hall conductivity patterns inferred from the TIROS-NOAA satellite data, *J. Geophys. Res.*, *92*, 7606-7618, 1987.

- Gonzales, C.A., M. C. Kelley and B. G. Fejer, Equatorial electric fields during magnetically disturbed conditions 2. Implications of simultaneous auroral and equatorial measurements, *J. Geophys. Res.*, **84**, 5803-5812, 1979.
- Hajj, G. A., R. Ibanez-Meier and E. R. Kursinski, Ionospheric imaging from a low Earth orbiter tracking GPS, in *Proc. GPS-93, Inst. of Navigation*, 1315-1322, 1993.
- Hajj, G. A., R. Ibanez-Meier, E. R. Kursinski and L. Romans, Imaging the Ionosphere with the Global Positioning System, *Int. J. Imaging. Sys. Tech.*, in press, 1994.
- Kelley, M. C., The Earth's ionosphere: plasma physics and electrodynamics, *Intl. Geophys. Ser.*, **43**, Academic Press, San Diego, 1989.
- Knipp, D. M., A. D. Richmond, G. Crowley, O. de la Beaujardiere, E. Friis-Christensen, D. S. Evans, J. C. Foster, I. W. McCrea, F. J. Rich, and J. A. Waldock, Electrodynamical patterns for September 19, 1984, *J. Geophys. Res.*, **94**, 16913-16923, 1989.
- Langel, R. A., 1974, Near-Earth magnetic disturbance in total field at high latitudes 1. Summary of data from Ogo 2, 4 and 6, *J. Geophys. Res.*, **79**, 2363-2371.
- Langel, R. A., R. H. Estes, G. D. Mead, E. B. Fabiano, and E. R. Lancaster, Initial geomagnetic field model from Magsat vector data, *Geophys. Res. Lett.*, **7**, 793-796, 1980.
- Langel, R. A. and R. H. Estes, Large-scale, near-Earth magnetic fields from external sources and the corresponding induced internal field, *J. Geophys. Res.*, **90**, 2487-2494, 1985.
- Langel, R. A., The Main Field, In: J. A. Jacobs, ed., *Geomagnetism, vol. 1*, Academic Press, 249-512, 1987.
- Langel, R. A., Global magnetic anomaly maps derived from POGO spacecraft data, *Phys. Earth. Plan. Int.*, **62**, 208-230, 1990.
- Langel, R. A., The use of low altitude satellite data bases for modeling of core and crustal fields and the separation of external and internal fields, *Surv. in Geophysics*, **14**, 31-87, 1993a.
- Langel, R. A., M. Purucker, and M. Rajaram, The equatorial electrojet and associated currents as seen in Magsat data, *J. Atmos. Terr. Phys.*, **55**, 1233-1269, 1993b.
- Mannucci, A. J., B. D. Wilson and C. D. Edwards, A new method for monitoring the Earth's ionospheric total electron content using the GPS global network, in *Proc. GPS-93, Inst. of Navigation*, 1323-1332, 1993.
- Matsushita, S. and B. Balsley, A question of DP-2, *Planet Space Sci.*, **20**, 1259-, 1972.
- Onwumechili, A., K. Kawasaki, and S.-I. Akasofu, Relationship between the equatorial electrojet and polar magnetic variations, *Planet Space Sci.*, **21**, 1, 1973.
- Rastogi, R. G., H. Chandra, R. P. Sharma, and G. Rajaram, Ground based measurements of ionospheric phenomena associated with the equatorial electrojet, *Indian J. Rad. Space Phys.*, **1**, 119-135, 1972.
- Ravat, D., and W. J. Hinze, Considerations of variations in ionospheric field effects in mapping equatorial lithospheric Magsat magnetic anomalies, *Geophys. Jour. Int.*, **113**, 387-398, 1993.
- Raymund, T. D., J. R. Austin, S. J. Franke, C. H. Liu, J. A. Klobuchar and J. Stalker, Application of computerized tomography to the investigation of ionospheric structures, *Radio Science*, **25**, 771-789, 1990.

- Raymund, T. D., S. E. Pryse, L. Kersley and J. A. T. Heaton, Tomographic reconstruction of the ionospheric electron density with European incoherent scatter radar verification, *Radio Sci.*, 28,, 811-817, 1993.
- Raymund, T. D., S. J. Franke and K. C. Yeh, Ionospheric Tomography: Its limitations and reconstruction methods, *J. Atmos. Terr. Phys.*, in press, 1994.
- Richmond, A. D., M. Blanc, B. A. Emery, R. H. Wand, B. G. Fejer, R. F. Woodman, S. Ganguly, P. Amayenc, R. A. Behnke, C. Calderon, and J. V. Evans, An empirical model of quiet-day ionospheric electric fields at middle and low latitudes, *J. Geophys. Res.*, 85, 4658, 1980.
- Richmond, A. D. and Y. Kamide, Mapping electrodynamic features of the high-latitude ionosphere from localized observations: techniques, *J. Geophys. Res.*, 93, 5741-5759, 1988.
- Richmond, A. D., Y. Kamide, B.-H. Ahn, S.-I. Akasofu, D. Alcayde, M. Blanc, O. de la Beaujardiere, D. S. Evans, J. C. Foster, E. Friis-Christensen, T. J. Fuller-Rowell, J. M. Holt, D. Knipp, H. W. Kroehl, R. P. Lepping, R. J. Pellinen, C. Senior, and A. N. Zaitzev, Mapping electrodynamic features of the high-latitude ionosphere from localized observations: combined incoherent-scatter radar and magnetometer measurements for January 18-19, 1984, *J. Geophys. Res.*, 93, 5760-5776, 1988.
- Richmond, A. D., Assimilative mapping of ionospheric electrodynamics, *Adv. Space Res.*, 12, 59-68, 1992.
- Rufenach, C. L., A radio scintillation method of estimating the small-scale structure in the ionosphere, *J. Atmos. Terr. Phys.*, 33, 1941, 1971.
- Rufenach, C. L., Power law wave number spectrum deduced from ionospheric scintillation observations, *J. Geophys. Res.*, 77, 4761, 1972.
- Salpeter, E. E., Interplanetary scintillation, I. Theory, *Astrophys. J.*, 147, 433, 1967.
- Srinivasan, J. M., T. K. Meehan and L. E. Young, Code and codeless ionospheric measurements with NASA's Rogue GPS receiver, in *Proc. GPS-89, Inst. of Navigation*, 451-453, 1989.
- Wilson, B. D., A. J. Mannucci, C. D. Edwards and T. Roth, Global ionospheric maps using a global network of GPS receivers, in *Proc. GPS-93, Inst. of Navigation*, 1343-1351, 1993.
- Woodman, R. F., Vertical drift velocities and east-west electric fields at the magnetic equator, *J. Geophys. Res.*, 75, 6249, 1970.
- Yanagisawa, M., and M. Kono, Mean ionospheric field correction for Magsat data, *J. Geophys. Res.*, 90, 2527-2536, 1985.

### Figure Captions.

Figure 1: Schematic illustration of a receiver in low-Earth orbit viewing a GPS satellite in an occultation geometry.

Figure 2: Map showing tangent points of GPS satellite occultations viewed by the aft-looking antenna on the GPS-MET satellite. In this example, over 200 occultations occur daily. The occultations tend to cluster in the mid-latitudes as a result of the geometry of the GPS satellite constellation.

Figure 3: Examples of electron density profiles reconstructed from simulated GPS signals propagated through a model ionosphere for four sample latitudes along 20°E longitude (Hajj et al., 1994). The true profiles (heavy lines) are derived from the Parameterized Ionosphere Model (PIM) of D. Anderson for noon on September 26, 1992. Open symbols: Profiles reconstructed only from the occultation data ; Solid symbols: Profiles derived with the aid of horizontal gradient information from ground network data. Note the underestimation at 0° and 20°N and overestimation at 40°N which is caused by proximity to the model's density maximum at 20°N. (a) 20°S; (b) 0°; (c) 20°N; (d) 40°N.

Figure 4: Model (heavy line) and reconstructed (broken line) electron density profiles for 40°S. In this example, the GPS profile reconstructed with the aid of ground data shows excellent agreement with the starting model, due to the gentle, linear gradient in the vicinity of the occultation tangent point.

Figure 5: Far left panels: Recovered electron density profiles (non-uniform) for 10°S, 0° and 10°N (broken lines) compared to PIM model (heavy line). These profiles differ from examples shown in Figure 3 by an adjustment that sets the profile minimum to zero. Middle panels: Conductivity estimates from the GPS electron density profiles shown at left.  $\sigma_o$ ,

Parallel conductivity ( $\times 10^{-4}$ );  $\sigma_p$ , Pedersen conductivity;  $\sigma_h$ , Hall conductivity;  $\sigma_c$ , Cowling conductivity ( $\times 10^{-2}$ ). Cowling conductivity calculated from the PIM model shown in heavy line for comparison to GPS-estimated  $\sigma_c$  (broken line). Far right panels: Zonal current density computed from the  $\sigma_c$  estimates for a .5 mV/m zonal electric field. Model shown in heavy line; GPS estimate in broken line.

Figure 6: Simulated distribution of high-resolution electron density profiles recovered during one day of Ørsted occultation data (800 x 400 km elliptical polar orbit). Plots are in magnetic latitude/local time coordinates. Symbols indicate the location of occultation tangent points, where high-resolution vertical profiles are resolved. (a) Northern hemisphere; (b) Southern hemisphere.

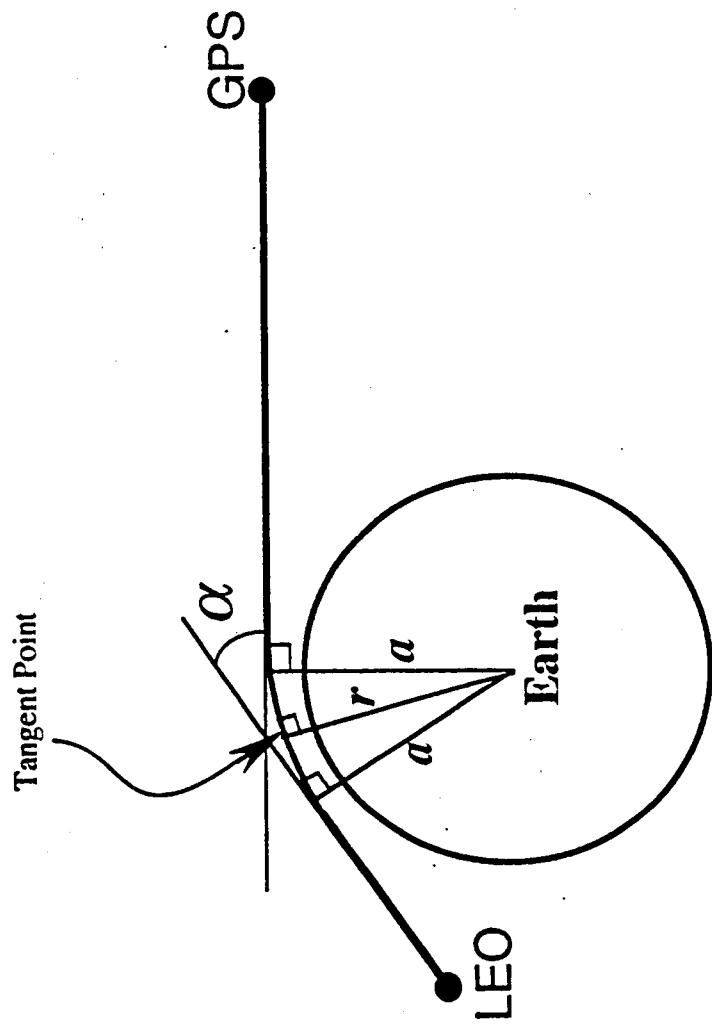


Figure 1

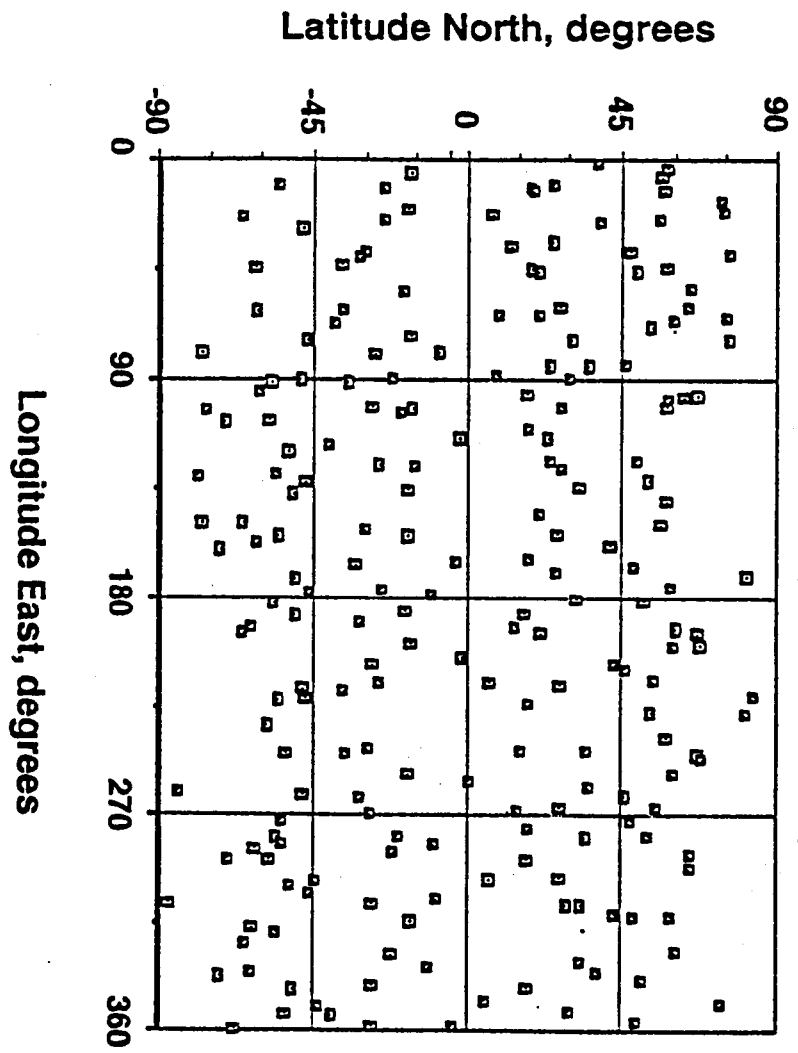
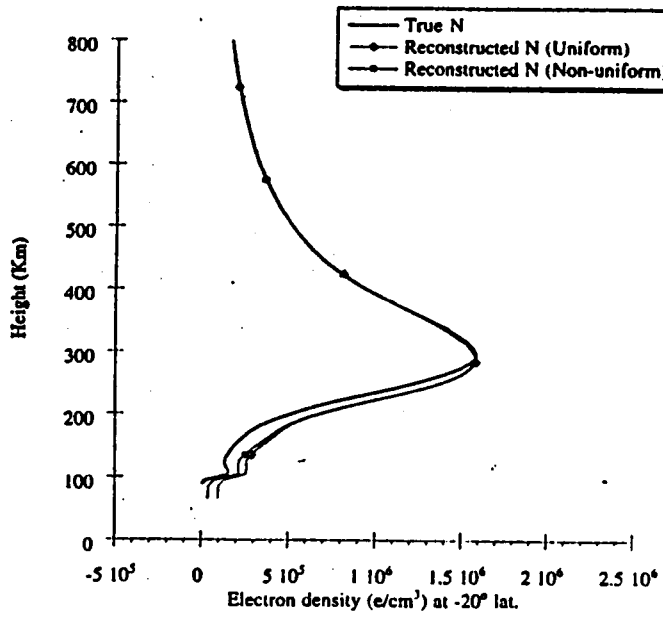
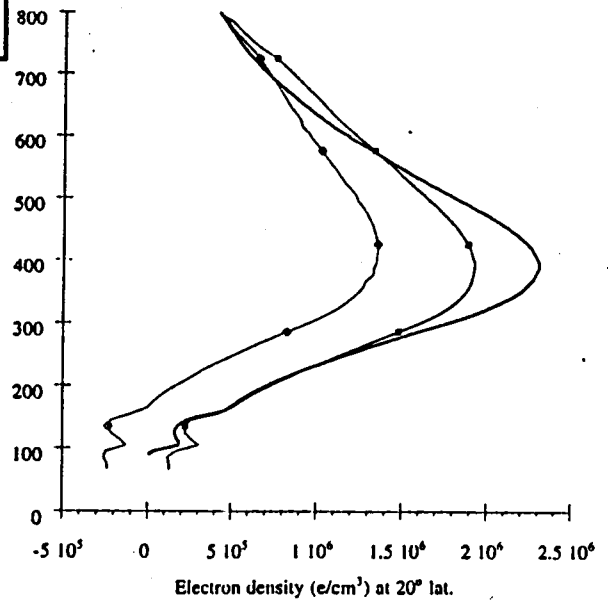


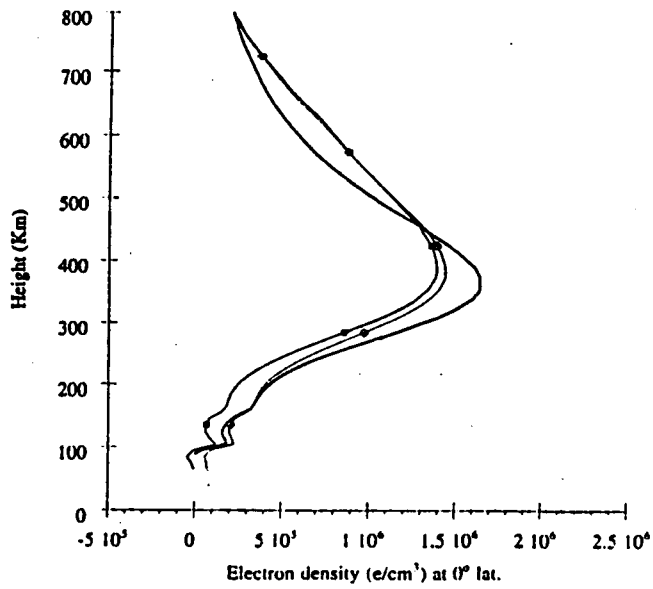
Figure 2.



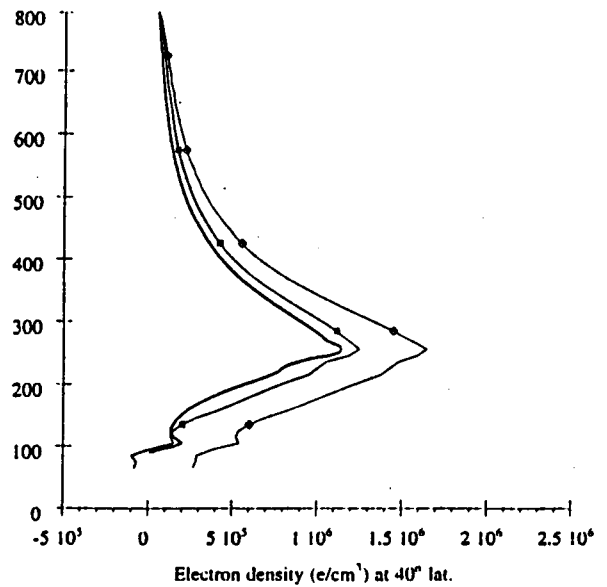
(a)



(c)



(b)



(d)

Figure 3.

### 40°S Electron Density

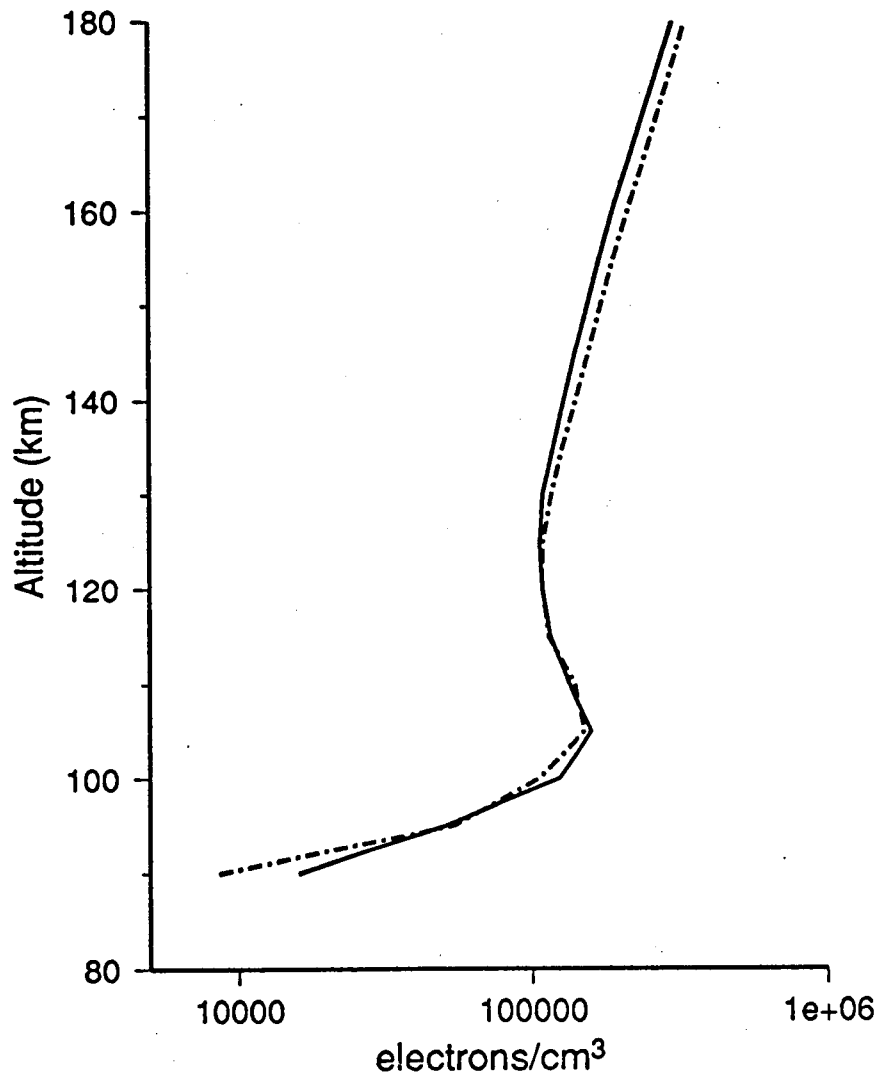


Figure 4.

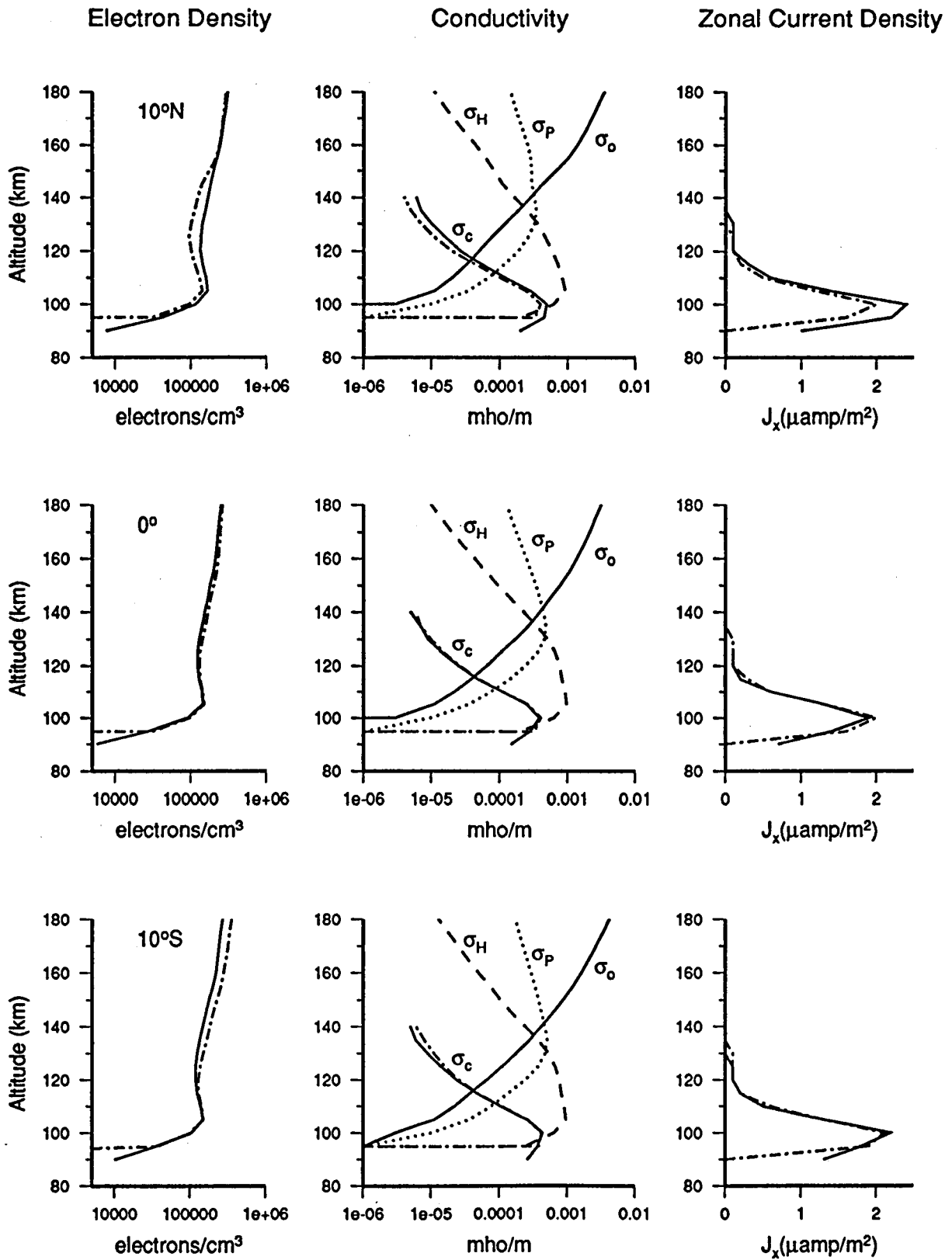


Figure 5.

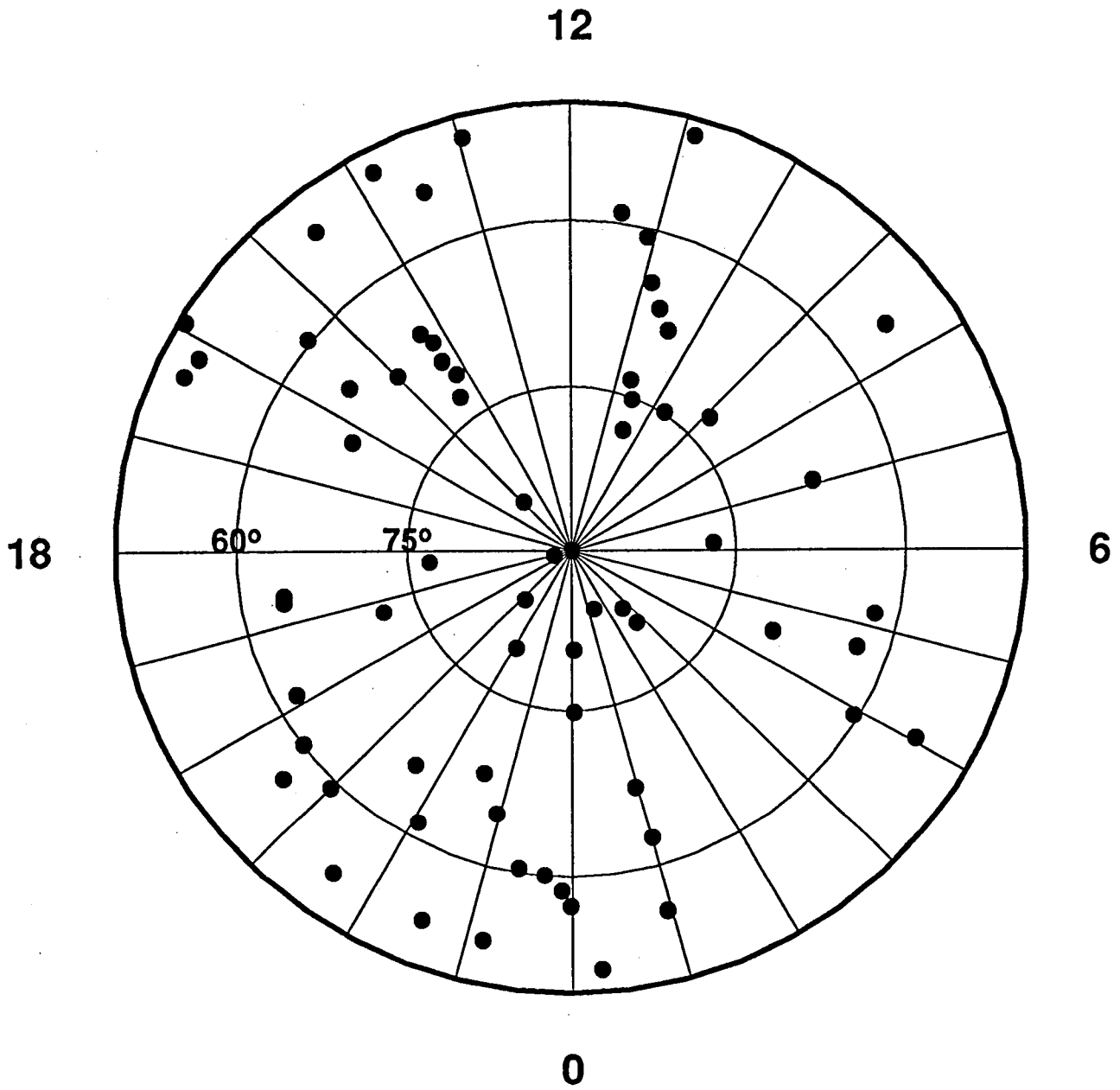


Figure 6a.

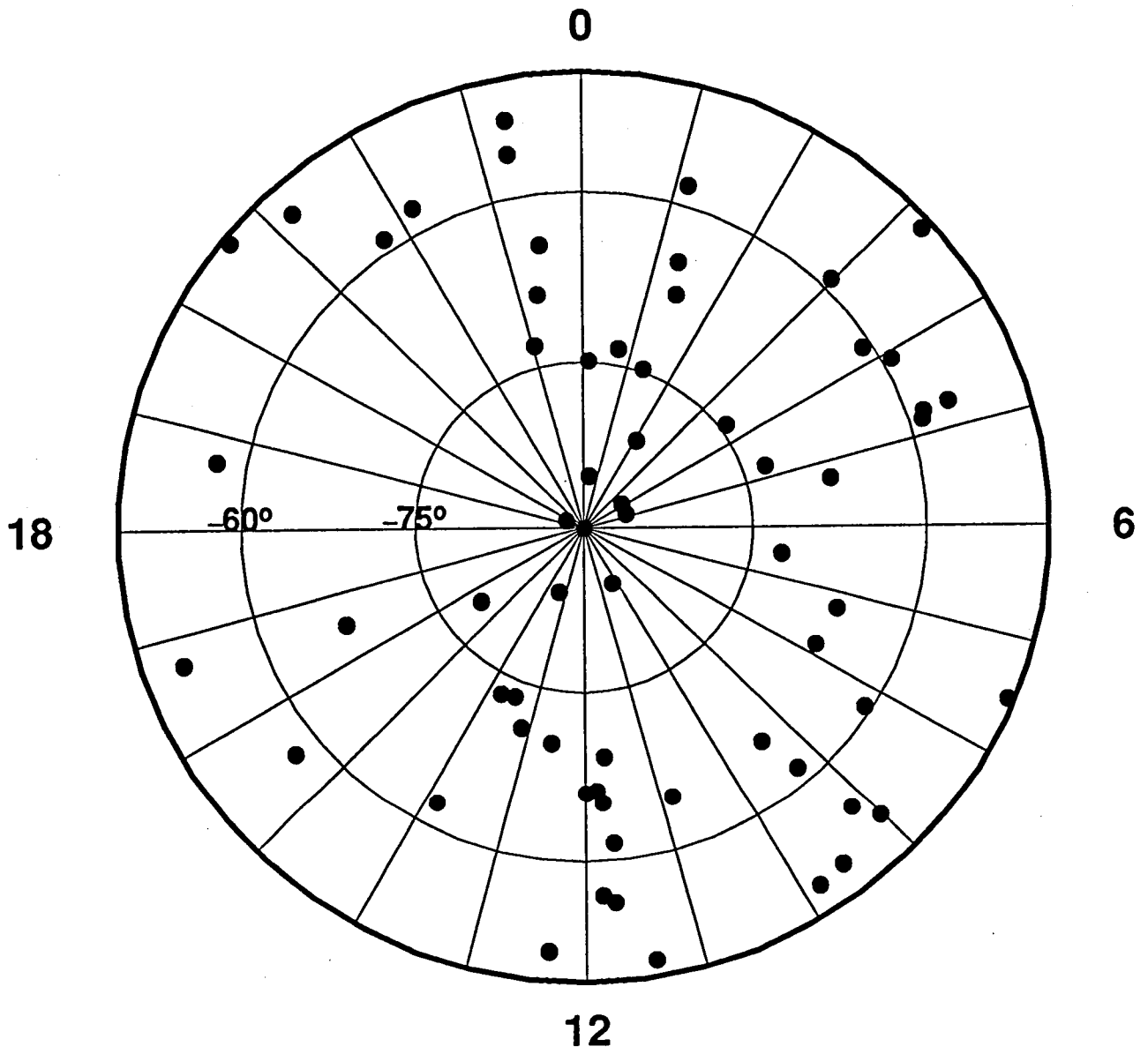


Figure 6b.